Journal of Applied Physics

Surface diffusion measurements of In on InGaAs enabled by droplet epitaxy

Cite as: J. Appl. Phys. **121**, 195302 (2017); https://doi.org/10.1063/1.4983257
Submitted: 02 February 2017 . Accepted: 27 April 2017 . Published Online: 16 May 2017

Margaret A. Stevens, Stephanie Tomasulo, Sergey Maximenko, Thomas E. Vandervelde, and Michael K. Yakes

Surface diffusion measurements of In on InGaAs enabled by droplet epitaxy

Margaret A. Stevens,[1] Stephanie Tomasulo,[2] Sergey Maximenko,[2]
Thomas E. Vandervelde,[1] and Michael K. Yakes[2,a)]
[1]*Department of Electrical Engineering, Tufts University, 161 College Avenue, Medford, Massachusetts 02155, USA*
[2]*Naval Research Laboratory, 4555 Overlook Avenue SW, Washington, DC 20375, USA*

(Received 2 February 2017; accepted 27 April 2017; published online 16 May 2017)

Surface diffusion is a critical parameter for non-equilibrium growth techniques such as molecular beam epitaxy. However, very little is known about diffusion rates of individual cations in a mixed cation material. Using droplet epitaxy as the growth technique, we isolate the diffusivity prefactor (D_0) and activation energy (E_A) of indium on the surface of $In_{0.53}Ga_{0.47}As$/InP(100). We report two regimes of indium diffusivity under As_2-rich conditions: above and below the droplet deposition temperature of 300 °C, corresponding to a change in surface reconstruction. We also discuss methods of extracting the indium diffusion parameters on metal-rich surfaces using droplet epitaxy and nucleation theory. The obtained diffusion parameters are compared to previous work in the literature and could be employed to optimize growth conditions for non-equilibrium crystal growth.
[http://dx.doi.org/10.1063/1.4983257]

I. INTRODUCTION

III-V compound semiconductors have been a key to developing a number of well-established optoelectronic technologies. Despite bulk miscibility gaps, many ternary and quaternary alloys can be grown with high material quality using non-equilibrium growth techniques such as molecular beam epitaxy (MBE) and metalorganic chemical vapor deposition (MOCVD). However, there exist several alloys where, despite the use of kinetically limited growth techniques, homogeneous alloys will decompose into smaller regions of more energetically favorable compounds. This process, known as phase separation, degrades the material properties and device performance, sometimes rendering them unusable. As demand for performance and design flexibility increases, device designs are calling for more and more use of challenging alloy systems. There have been several technologically important III-V ternary and quaternary alloys afflicted by phase separation, including but not limited to InGaAs,[1] InGaP,[2] GaAsSb,[3] InAsSb,[4] and InGaAsP.[5]

The separation of immiscible alloy phases occurs as the system reaches thermodynamic equilibrium. Achieving such an equilibrium condition, however, is limited by kinetics. For bulk materials, the kinetic path to phase separation is solid state diffusion. Unlike the mechanisms of bulk phase separation, which are largely well understood, the physics of surface-mediated phase separation is largely immature. This is due to the lack of information regarding diffusion barriers involved in semiconductor growth as well as available techniques required to characterize phase separated materials at the atomic scale. While analytical models have been proposed to link surface diffusion with the appearance of phase separation,[6,7] practical implementation of these models depends on the availability of surface diffusion parameters such as the diffusivity prefactor (D_0) and the activation energy (E_A) of the growth atoms. Information about these parameters on a mixed cation surface is extremely limited because until recently, no available technique could differentiate individual cation diffusion lengths in a mixed cation alloy.

Recently, Bietti *et al*. used droplet epitaxy to directly measure the gallium diffusion length on a GaAs surface.[8] This process involves depositing group-III droplets directly on the alloy surface in a group-V purged environment, then crystallizing the droplets into 3D structures by exposing the surface to a group-V overpressure.[9] Droplet epitaxy enables access to the diffusion parameters because the radius of a "halo" of material that surrounds the group-III droplet is directly related to the diffusion length of the group-III cation.[8,10,11] Anisotropic surface diffusion of indium on InGaAs at the InP lattice constant has been shown at temperatures below 300 °C, but the diffusivity has yet to be characterized quantitatively.[12] Additionally, exploring increased deposition temperatures (up to 500 °C) is advantageous as higher temperatures move closer towards the growth-space of the underlying InGaAs layer, allowing the diffusion measurements to accurately reflect bulk ternary growth.

In this paper, we employ droplet epitaxy to isolate the diffusivity parameters for indium on the surface of $In_{0.53}Ga_{0.47}As$/InP under As-rich conditions and over a large range of deposition temperatures (200–495 °C), as well as describe a pathway to identifying these parameters on a metal-rich surface. We find two regimes of diffusivity behavior in the As-rich condition: above and below 300 °C, with [011] as the fast-diffusion direction. Concurrently with this change in diffusivity behavior, we observe a change in diffusion halo morphology. Above 300 °C, quantum dots (QDs) appear in the diffusion halo, which we believe to be formed by Stranski-Krastanov (S-K) growth processes when the diffusion halos achieve a critical thickness. We attribute the change in diffusivity to a change in surface reconstruction brought on by increasing droplet deposition temperature. This experiment can be generalized to identify the individual cation diffusion lengths on any ternary or quaternary material system to mitigate surface-mediated phase separation in III-V alloys.

a)Electronic mail: michael.yakes@nrl.navy.mil

TABLE I. List of droplet diffusion samples. Arsenic flux rate (J'_{As}) normalized to a nominal flux of 2 ML/s and indium flux rate (J'_{In}) normalized to an anticipated rate 0.15 ML/s.

Sample ID	Droplet T (°C)	J'_{As}	J'_{In}
T495	495	1	1.0
T400	400	1	1.0
T350	350	1	1.0
T300	300	1	1.0
T250	250	1	1.0
T200	200	1	1.0
F1	200	0	1.0
F2	300	1/2	1.0
F3	300	1/4	1.0
F4	200	1	2.0
F5	200	1	3.5

II. EXPERIMENTAL

The structures explored in this study were grown on a Riber Compact 21 DZ MBE system. Sample IDs, droplet deposition temperatures, and flux information are listed in Table I. Temperatures were measured by a thermocouple and are in reference to the InP (2×4) to (4×2) reconstruction transition under As_2-overpressure, which occurred at $519\pm5\,^{\circ}C$ for our system. All samples were grown on epi-ready InP(100) substrates with a 2° offcut along a direction that is 45° away from both [011] and $[0\bar{1}1]$, purchased from Wafer Technology, Ltd. The oxide was removed by heating the substrate to the (2×4) to (4×2) transition under As_2-overpressure and immediately quenched to $499\pm5\,^{\circ}C$ to grow 0.5 μm of $In_{0.53}Ga_{0.47}As$, using the RHEED system to monitor and ensure smooth 2D growth. The InGaAs layers were grown under identical conditions for every sample, utilizing a V/III beam equivalent pressure ratio of ~5 and demonstrating a streaky (2×4) surface reconstruction during growth.

After the bulk growth, the indium and gallium shutters were closed, and the substrate was cooled to the desired droplet deposition temperature, ranging from 200 to 495 °C under As_2 overpressure. Once the temperature stabilized, the As valve and shutter were closed, and the growth was paused until system pressure asymptoted to roughly 5×10^{-9} T. After the system was purged of As, the indium shutter was opened to deposit ~5 ML of indium at a flux rate of 0.15 ML/s to form droplets in a Volmer-Weber-like fashion.[13] Next, the indium shutter was closed, and the As shutter and valve were immediately opened to crystallize the droplets, under an As_2 flux of $\sim8\times10^{-6}$ T, corresponding to a nominal growth rate of ~2 ML/s for 2 min. The RHEED reconstruction transitioned back to a (2×4) or (4×3) pattern, depending on the droplet deposition temperature. After crystallization, the samples were cooled under As_2 flux and removed from the MBE chamber for characterization.

A Rigaku SmartLab X-ray diffraction system was utilized to confirm composition and thickness of the underlying InGaAs layer. Atomic force microscopy (AFM) images were used to measure diffusion halos and were taken using either the Bruker Dimension FastScan system or the Asylum Cypher S system in tapping mode in air. Images were analyzed using the open-source SPM program Gwyddion.[14] Scanning electron microscopy (SEM) images were used to quantify nucleation densities and were taken using a Zeiss Ultra Plus SEM.

III. RESULTS AND DISCUSSION

Figure 1 shows select AFM images of our samples, both without (Figure 1(a)) and with (Figures 1(b)–1(e)) the arsenic crystallization step. At the lowest temperature, 200 °C, the diffusion ring around the indium droplet is nearly symmetrical. As the droplet deposition temperature increases, we see the diffusion halo expand anisotropically, longer along [011] than $[0\bar{1}1]$. Our droplets appear to etch into the InGaAs underlying layer during the As crystallization stage as previously demonstrated in the literature for InAs/InGaAs structures.[11,15] At droplet deposition temperatures above 300 °C, we see QD formation in the diffusion halo, which has been previously documented in the literature for InAs/InGaAs/

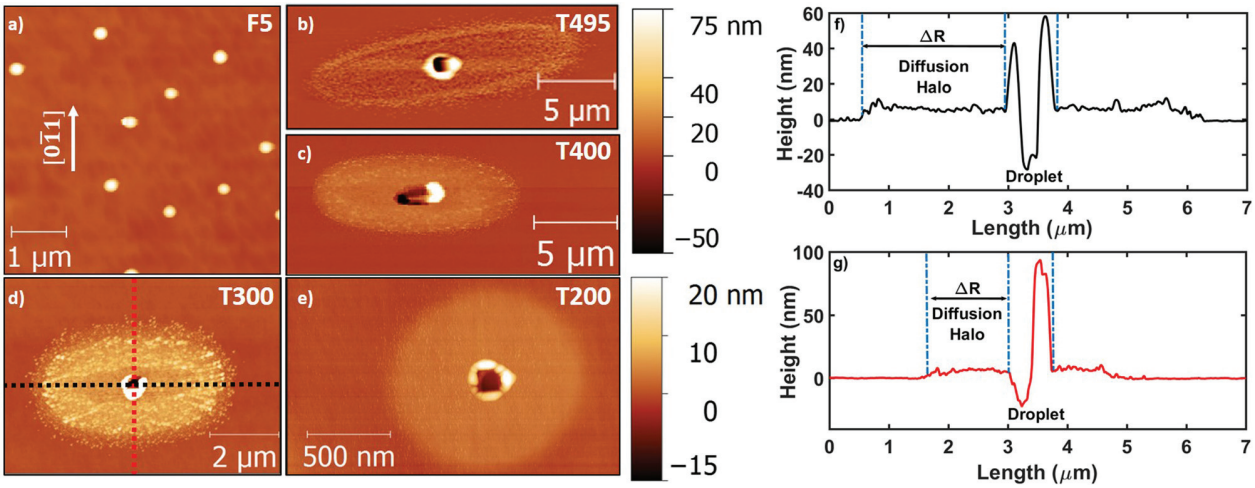

FIG. 1. (Left) AFM images of selected samples: (a) F5 (no As flux), (b) T495, (c) T400, (d) T300, and (e) T200. (Right) AFM profiles of T300 structure along the (f) [011] and (g) $[0\bar{1}1]$ directions with labels indicating the regions that constitute the InAs diffusion halo and the indium droplet.

GaAs structures[16] but to the best of our knowledge has not been shown for the less-strained InAs/InGaAs/InP structure.

AFM profiles of T300 are also shown in Figures 1(f) and 1(g), indicating that we measure the diffusion halo (ΔR) in a similar fashion to previous work on diffusion measurements enabled by droplet epitaxy.[8,10] ΔR is related to the diffusion parameters by the following equation:[8]

$$\Delta R = \ell = \sqrt{D_0 e^{\frac{-E_A}{k_B T}} 1/J_{As}}, \quad (1)$$

where ℓ is the diffusion length (cm), D_0 is the diffusivity prefactor (cm^2/s), E_A is the activation energy (eV), k_B is Boltzmann's constant (eV/K), T is the droplet deposition temperature (K), and J_{As} is the normalized As flux (ML/s).

Figure 2 shows the Arrhenius fit of our data to Equation (1). As expected, we find that diffusion increases with increasing temperature, and decreases with increasing As-flux. Our work finds that the rate of change of the diffusion length decreases above 300 °C, yielding "high temperature" and "low temperature" diffusion parameters in addition to the differences along the [011] and $[0\bar{1}1]$ crystallographic directions. The computed diffusion parameters are listed in Table II. We find that the temperature variation and our As-flux variation (performed right at the transition temperature T = 300 °C) experiments yield parameters that are in good agreement with each other. We extracted D_0 from the fitting parameter in the As-flux data by using the high temperature values for E_A, due to T300 having morphological (Figure 1(d)) and surface reconstruction (Figures 4(c) and 4(d)) characteristics of our other high temperature samples.

TABLE II. Computed diffusion parameters from data in Figure 2. D_0 for As-flux experiments extracted from fitting parameter by using the high temperature value for E_A. Error on fitting parameters represents one standard deviation on the fit, or 68% confidence values.

	D_0 (cm^2/s)	E_A (eV)
High-T	[011]: $6.4(\pm 2.0) \times 10^{-3}$	[011]: 0.55 ± 0.02
	$[0\bar{1}1]$: $1.89(\pm 1) \times 10^{-6}$	$[0\bar{1}1]$: 0.20 ± 0.03
Low-T	[011]: $9.1(\pm 7.7) \times 10^{-2}$	[011]: 0.68 ± 0.04
	$[0\bar{1}1]$: $2.4(\pm 1.8) \times 10^{-3}$	$[0\bar{1}1]$: 0.54 ± 0.03
As-Flux	[011]: $6.5(\pm 5.0) \times 10^{-3}$	…
	$[0\bar{1}1]$: $1.72(\pm 0.8) \times 10^{-6}$	…

To explore the dependence of the halo morphology on temperature, we used AFM to analyze the height profiles of the diffusion halos. Figure 3 shows the height of the diffusion halos for temperatures ranging from 200 to 495 °C, with the outer diameter of the halos normalized for viewing convenience. If the QDs are formed by a S-K growth process, we can think of the diffusion halo region as a "wetting layer" for QD formation. Previous work on the transition between 2D and 3D growth of InAs on a lattice-matched InGaAs/InP surface found the critical thickness of the wetting layer decreased dramatically with increasing deposition temperature.[17] While the critical thickness for the formation of QDs decreases with increasing temperature, Figure 3 shows the thickness of the diffusion halo increased with increasing temperature (T200, T250, and T300). At the droplet deposition temperatures above T = 300 °C, we see QD formation in the diffusion halo. This is shown in the AFM images in Figure 1 and is evident in the roughening of the T300, T400, and T450 profiles in Figure 3. We can estimate the critical thickness for S-K QD formation is somewhere between 6–8 nm for T = 300 °C, as T250 has a diffusion halo thickness

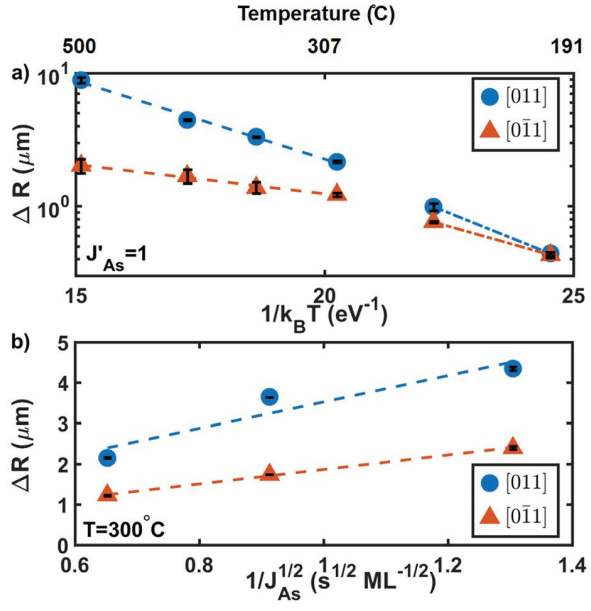

FIG. 2. (a) Diffusion length (ΔR) as a function of droplet deposition temperature along the [011] and $[0\bar{1}1]$ directions. Data are fit according to an Arrhenius relationship derived by Bietti *et al.*[8] Error bars indicate one standard deviation. A difference in fitting parameters above and below 300 °C indicates a change in surface kinetics and a surface phase transition between 250 and 300 °C. (b) Diffusion length (ΔR) fit to normalized arsenic flux for samples T300, F2, and F3, all grown at 300 °C.

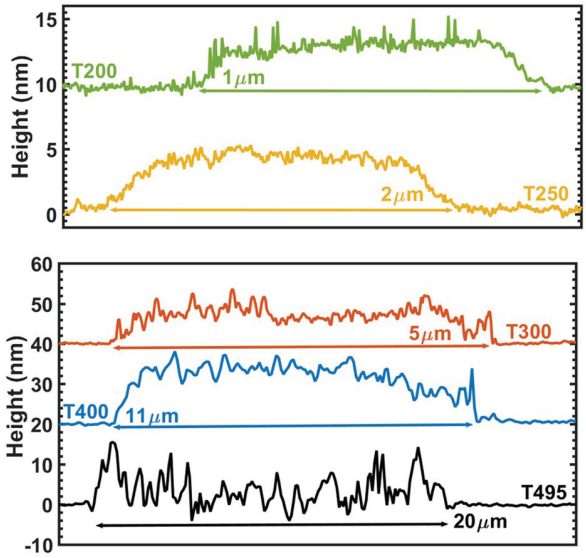

FIG. 3. Diffusion halo height for various droplet deposition temperatures, measured just above the indium droplets and characterized by AFM. Profiles plotted with the height's zero level offset and the outer diameter normalized to aid with comparison. Double arrows indicate approximate outer diameter of each diffusion halo. In order from top to bottom: T200, T250, T300, T400, and T500.

of 5 nm and yields no QDs, and T300 has a thickness of 8–12 nm, with roughening due to QD formation.

We find the temperature that yields diffusion halos that exceed S-K critical thickness is highly dependent on the group-V flux as well. Although we see QD formation for T300, we did not see QD formation in growth conditions with reduced As-flux (F2 and F3) despite observing the high temperature (2×4) reconstruction. This indicates that the changing diffusion coefficient observed in Figure 2 is primarily due to the changing surface reconstruction and not due to the onset of quantum dot formation.

The abrupt change in D_0 and E_A as a function of temperature can be linked to a change in surface reconstruction.[18] Figure 4 depicts RHEED reconstructions at two critical steps in droplet epitaxy. Figures 4(a) and 4(b) show the [011] and $[0\bar{1}1]$ reconstructions during indium deposition. A (4×2) reconstruction, indicating a metal-rich surface, is present regardless of deposition temperature. Figures 4(c) and 4(d) show the (2×4) reconstruction during arsenic crystallization, using T400 as an example. At droplet deposition temperatures below 300 °C, a change in reconstruction occurs during crystallization. Figures 4(e) and 4(f) show the (4×3) reconstruction, using T250 as an example. The (4×3) reconstruction is known to be typical for $In_{0.53}Ga_{0.47}As$/InP growth.[19]

Mirecki Millunchick *et al*. explored a change in the surface reconstruction of InGaAs on InP resulting from a change in composition.[19] STM images and RHEED reconstructions showed lattice matched $In_{0.53}Ga_{0.47}As$/InP has a (4×3) reconstruction, when grown under conditions that maintain layer-by-layer growth. Lattice mismatched structures, such as $In_{0.81}Ga_{0.19}As$/InP, show a (2×4) reconstruction, similar to bulk InAs or bulk GaAs. Xun *et al*.[20] documents the RHEED transitions for InGaAs on GaAs as a function of substrate temperature, highlighting a transition from $(4 \times 3)/(n \times 3)$ to (2×4) under increasing As-overpressure. They attribute these changes in surface reconstruction to indium segregation and eventually desorption. Regardless of mechanism, the change in surface reconstruction that we see is indicative of a change in surface kinetics.

During the droplet deposition step, the first monolayer of deposited indium is consumed by the underlying InGaAs layer, transforming it from an As-terminated to an indium-terminated surface.[21] We see evidence of this almost instantaneously with the RHEED, as the surface reconstruction transitions to (4×2) pattern immediately after the indium shutter is opened. Next, the incident indium atoms diffuse on the group-III terminated surface, colliding, accumulating, and dispersing until they reach the critical cluster size and become stable.[21] Therefore, the surface density of the droplets, their size, and their spacing could be related to a diffusivity prefactor through classical nucleation theory.[21,22]

We measure the droplet density of our samples through SEM imaging, as shown in Figure 5(a). Figure 5(b) depicts the indium droplet density as a function of indium flux rate for samples T200, F4, and F5. As expected, the droplet density increases with increasing indium flux, at T = 200 °C. Figure 5(c) shows the surface density of droplets as a function of deposition temperature for samples. Previous work in the literature has shown the formation of group-III metal droplets on a III-V surface is highly temperature dependent[24] and has an Arrhenius relationship at droplet deposition temperatures below 300 °C.[10,21]

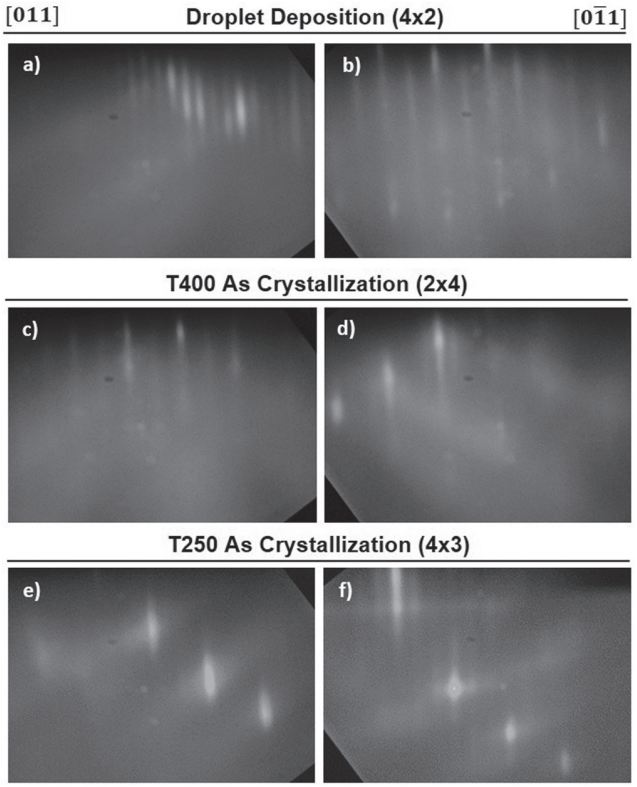

FIG. 4. RHEED reconstruction of samples along [011] and $[0\bar{1}1]$ azimuthal directions. (a) and (b) (4×2) reconstruction from T400 during indium droplet deposition, present for all droplet deposition temperatures. (c) and (d) (2×4) reconstruction of T400 sample during arsenic crystallization. (e)–(f) (4×3) reconstruction from T250 sample during As crystallization. Reconstruction appears to change around the temperature where the diffusion coefficients change.

Most work involving nucleation theory is done with T < 300 °C to deactivate many thermal processes. This is a result of the diffusion coefficient being more complexly related to temperature than it is for diffusion halo measurements[22] and the onset of cluster density evolution due to processes like Ostwald ripening.[21] However, Figure 5(c) shows the droplet density as a function of deposition temperature has an Arrhenius fit at temperatures above 300 °C. We saw a (4×2) surface reconstruction for all samples during the droplet deposition step, as shown in Figures 4(a) and 4(b) for T400. We also note that we do not find a difference in our fit due to coarsening by Ostwald ripening that has been observed in gallium droplet epitaxy on GaAs substrates.[21] This is consistent with previous work on indium droplet epitaxy on InP up to 300 °C.[10] Further investigation on nucleation theory may be able to relate the fitting parameters shown in Figure 5(c) to a diffusivity prefactor to analyze the cation diffusion parameters on the indium rich (4×2) surface. As Figure 2(a) shows that diffusion is highly dependent on surface reconstruction, it would be of interest to analyze any change in diffusion parameters that arise during the different steps of MBE growth.

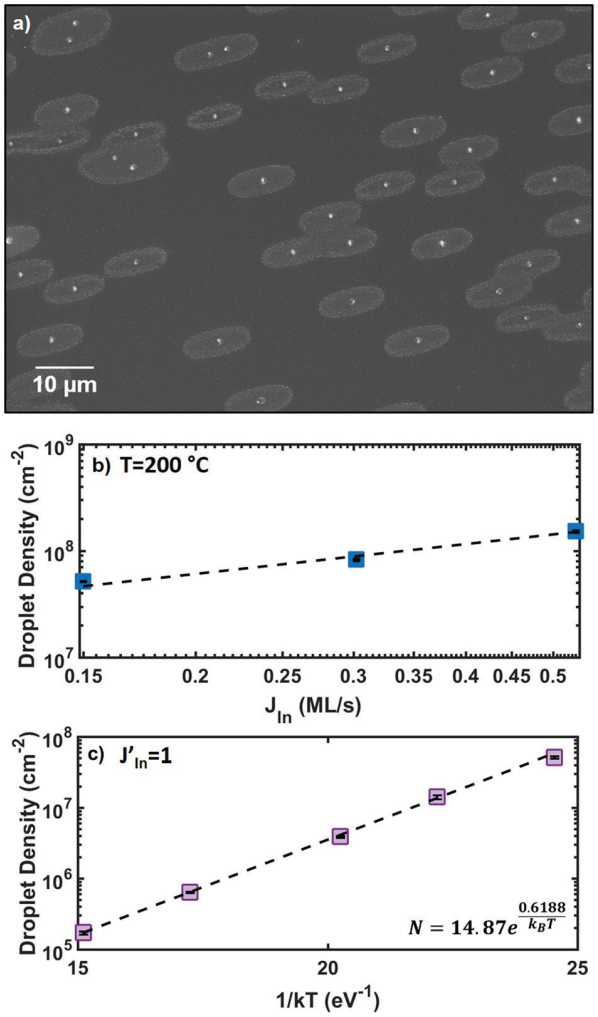

FIG. 5. (a) SEM image of T400. (b) Droplet density per surface area as a function of indium flux during the droplet deposition step. (c) Droplet density per surface area as a function of droplet deposition temperature. Data fit the Arrhenius relationship for nucleation theory.[21,23]

Table III compares our work to previous experiments on diffusion parameters in the literature. Early work in this field used a variety of methods to extract diffusion parameters ranging from completely theoretical examinations[26–28] to complex scanning tunneling microscopy (STM) experiments.[27] Since 2014, more groups have explored droplet epitaxy as a method to extract important diffusion parameters. However, most previous work explored droplet deposition temperatures below 350 °C, significantly lower than the bulk material growth temperature. We find that our work aligns well with the work of Fuster *et al.*[10] and Noda *et al.*[11] although we see a significantly faster diffusion rate along the [011] direction in both the high-T and low-T cases. For the [011] direction, our work falls closer to that of Bietti *et al.*[8] in terms of both D_0 and E_A. The direction of anisotropy in our structures is consistent with previous work of indium diffusion in InGaAs strained on GaAs[11,16] and low-temperature work of droplet epitaxy of indium on InGaAs/InP,[12] but the opposite direction of the reported work with indium diffusion directly on InP.[10] Previous studies on the reconstruction of InP(001) under As-overpressure at temperatures above 350 °C show a (4×2) surface reconstruction. This is the opposite orientation of the surface reconstructions we see at high droplet deposition temperatures (shown in Figure 4[29,30]), further confirming the influence of surface reconstruction on diffusion parameters. This change in anisotropy shows that researchers can influence both the magnitude and direction of cation surface diffusion by choice of growth conditions that manipulate the surface reconstruction.

IV. CONCLUSIONS

By employing droplet epitaxy as our deposition technique, we successfully extracted the surface diffusion parameters for indium on the surface of $In_{0.53}Ga_{0.47}As$/InP(100) in an As_2-rich environment, as well as analyzed the nucleation

TABLE III. Examples of diffusivity prefactors and activation energies in literature, shown in chronological order.

References	Material system	D_0 (cm^2/s)	E_A (eV)	Method
25	GaAs/GaAs	$0.85(\times 3.88^{\pm 1}) \times 10^{-5}$	1.3 ± 0.1	RHEED
26	GaAs/GaAs	1.637×10^{-5}	0.101	Simulation
	InAs/GaAs	1.251×10^{-5}	0.073	
27	GaAs/GaAs	0.2	1.0 ± 0.1	Simulation/STM
28	InAs/InGaAs/GaAs	10^{-4}–10^{-5}	[110]: 0.8–1.0	Simulation: KMC
			$[1\bar{1}0]$: 0.4–0.9	and DFT
11	InAs/GaAs	(not provided)	[011]: 0.34	Droplet epitaxy
			$[0\bar{1}1]$: 0.21	
8	GaAs/GaAs	$0.53(\times 2.1^{\pm 1})$	1.31 ± 0.15	Droplet epitaxy
10	InAs/InP	[011]: $1.5(\pm 0.4) \times 10^{-6}$	[011]: 0.28 ± 0.01	Droplet epitaxy
		$[0\bar{1}1]$: $0.4(\pm 0.14) \times 10^{-6}$	$[0\bar{1}1]$: 0.25 ± 0.02	
Our work	InAs/InGaAs/InP	High-T	High-T	Droplet epitaxy
		[011]: $6.4(\pm 2.0) \times 10^{-3}$	[011]: 0.55 ± 0.02	
		$[0\bar{1}1]$: $1.89(\pm 1.0) \times 10^{-6}$	$[0\bar{1}1]$: 0.20 ± 0.03	
		Low-T	Low-T	
		[011]: $9.1(\pm 7.7) \times 10^{-2}$	[011]: 0.68 ± 0.04	
		$[0\bar{1}1]$: $2.4(\pm 1.8) \times 10^{-3}$	$[0\bar{1}1]$: 0.54 ± 0.03	

density as a function of droplet deposition temperature as a link to surface diffusion on a metal-rich surface. In the As_2-rich environment, we identified two different regimes of diffusion behavior above and below the droplet deposition temperature of 300 °C. A change in the RHEED reconstruction around this droplet deposition temperature signaled a change in the surface kinetics. The onset of the QDs in the diffusion halo at 300 °C appeared to be a result of a S-K growth process, with the diffusion halos acting as a wetting layer and reaching the critical thickness to form quantum dots. Next, we employed nucleation theory to discuss group-III cation diffusion on a metal-rich surface using droplet epitaxy and nucleation theory. We showed that droplet surface density as a function of temperature has an Arrhenius fit and does not show behavior indicative of Ostwald ripening, even at a maximum droplet deposition temperature of $T = 495$ °C. This is in good agreement with previous droplet epitaxy work of In/InP up to 350 °C. Finally, we compiled previous surface diffusion measurements in the literature and compared the magnitude of cation surface diffusion as well as preferred diffusion direction on different III-V surfaces. By employing an experiment that isolates one cation's diffusion parameters in a mixed group-III ternary material, we develop a path to better understanding the factors behind phase separation in MBE grown III-V materials.

ACKNOWLEDGMENTS

This work was supported by the Office of Naval Research. M.A.S. acknowledges support from the NASA Space Technology Research Fellowship (NSTRF). This work was performed in part at the Center for Nanoscale Systems (CNS), a member of the National Nanotechnology Coordinated Infrastructure Network (NNCI), which was supported by the National Science Foundation under NSF Award No. 1541959. CNS is part of Harvard University.

[1]N. J. Quitoriano and E. A. Fitzgerald, J. Appl. Phys. **102**, 033511 (2007).
[2]S. Tomasulo, J. Simon, P. J. Simmonds, J. Biagiotti, and M. L. Lee, J. Vac. Sci. Technol. B: Microelectron. Nanometer Struct. **29**, 03C118 (2011).
[3]Y. R. Chen, L. C. Chou, Y. J. Yang, and H. H. Lin, Thin Solid Films **520**, 4486 (2012).
[4]H. Miyoshi, R. Suzuki, H. Amano, and Y. Horikoshi, J. Cryst. Growth **237–239**, 1519 (2002).
[5]L. Ji, M. Tan, K. Honda, R. Harasawa, Y. Yasue, Y. Wu, P. Dai, A. Tackeuchi, L. Bian, S. Lu, and H. Yang, Sol. Energy Mater. Sol. Cells **137**, 68 (2015).
[6]I. Ipatova, V. Malyshkin, a. Maradudin, V. Shchukin, and R. Wallis, Phys. Rev. B **57**, 12968 (1998).
[7]E. Luna, M. Wu, J. Puustinen, M. Guina, and A. Trampert, J. Appl. Phys. **117**, 185302 (2015).
[8]S. Bietti, C. Somaschini, L. Esposito, A. Fedorov, and S. Sanguinetti, J. Appl. Phys. **116**, 114311 (2014).
[9]N. Koguchi and K. Ishige, Jpn. J. Appl. Phys. **32**, 2052 (1993).
[10]D. Fuster, K. Abderrafi, B. Alén, Y. González, L. Wewior, and L. González, J. Cryst. Growth **434**, 81 (2016).
[11]T. Noda, T. Mano, and H. Sakaki, Cryst. Growth Des. **11**, 726 (2011).
[12]T. Noda, T. Mano, M. Jo, T. Kawazu, and H. Sakaki, J. Appl. Phys. **112**, 063510 (2012).
[13]J. Wu and Z. M. Wang, J. Phys. D: Appl. Phys. **47**, 173001 (2014).
[14]D. Nečas and P. Klapetek, Open Phys. **10**, 181 (2012).
[15]T. Noda, M. Jo, T. Mano, T. Kawazu, and H. Sakaki, J. Cryst. Growth **378**, 529 (2013).
[16]T. Noda and T. Mano, Appl. Surf. Sci. **254**, 7777 (2008).
[17]M. Gendry, V. Drouot, C. Santinelli, and G. Hollinger, Appl. Phys. Lett. **60**, 2249 (1992).
[18]J. S. Kim, Mater. Sci. Semicond. Process. **57**, 70 (2017).
[19]J. M. Millunchick, A. Riposan, B. J. Dall, C. A. Pearson, and B. G. Orr, Surf. Sci. **550**, 1 (2004).
[20]Z. Xun, L. Zi-Jiang, G. Xiang, Z. Bi-Chan, S. Lin-Tao, Z. Qing, D. Chao-Yong, and D. Zhao, Chin. Phys. B **21**, 046103 (2012).
[21]C. Heyn, A. Stemmann, A. Schramm, H. Welsch, W. Hansen, and Á. Nemcsics, Phys. Rev. B - Condens. Matter Mater. Phys. **76**, 075317 (2007).
[22]J. A. Venables, G. D. T. Spiller, and M. Hanbucken, Rep. Prog. Phys. **47**, 399 (1984).
[23]H. Brune, G. S. Bales, J. Jacobsen, C. Boragno, and K. Kern, Phys. Rev. B **60**, 5991 (1999).
[24]J. H. Lee, Z. M. Wang, and G. J. Salamo, J. Phys. Condens. Matter **19**, 176223 (2007).
[25]J. H. Neave, P. J. Dobson, B. A. Joyce, and J. Zhang, Appl. Phys. Lett. **47**, 100 (1985).
[26]A. Palma, E. Semprini, A. Talamo, and N. Tomassini, Mater. Sci. Eng. B **37**, 135 (1996).
[27]V. P. LaBella, D. W. Bullock, Z. Ding, C. Emery, W. G. Harter, and P. M. Thibado, J. Vac. Sci. Technol. A: Vac., Surf., Films **18**, 1526 (2000).
[28]M. Rosini, M. C. Righi, P. Kratzer, and R. Magri, Phys. Rev. B - Condens. Matter Mater. Phys. **79**, 075302 (2009).
[29]Y. J. Chun, T. Sugaya, Y. Okada, and M. Kawabe, Jpn. J. Appl. Phys. **32**, 287 (1993).
[30]S. Ohkouchi and I. Tanaka, Appl. Phys. Lett. **59**, 1588 (1991).